Transverse Momentum in Nucleons, From Raw Data to TMD Model Extraction

David M. Riser

June 2018

Contents

1 Motivation

1.1 Statement of Purpose

This dissertation will present measurements for,

1. the SIDIS structure function combination $F_{UU,T} + \epsilon F_{UU,L}$, as well as the structure function $F_{UU}^{\cos\phi}$, and $F_{UU}^{\cos(2\phi)}$. These quantities will be extracted for π^+ and π^- from the differential cross section.

2. the SIDIS structure function $F_{LU}^{\sin\phi}$. This will be extracted from beam spin asymmetry measurements for K^+.

Finally, using these results, the last chapter of my dissertation will be devoted to a phenomenological analysis of the results in the framework of TMD functions. This work will take place as a collaboration between myself and the EVA working group.

1.2 Qualitative Motivation

The field of nuclear and particle physics grew tremendously during the middle part of the 20th century. As the Stanford Linear Accelerator (SLAC) accelerated electrons and collided them into various types of targets, previously unknown particles were discovered rapidly. The abundance of particles was eventually explained by Gell-Man and Zweig with the inclusion of a set of new fundamental particles called quarks that carried a new degree of freedom known as color. These ideas birthed the Quark Model which successfully predicted the masses and existence of new particles made of quarks, and eventually grew into Quantum Chromodynamics (QCD).

A key feature of Quantum Chromodynamics is confinement; bound states of quarks must be colorless and thus quarks cannot be directly observed outside of the hadrons they compose. During the last 50 years, quark momenta within hadrons has been studied successfully with co-linear parton distribution functions (PDFs). At leading order these functions $f(x)$ can be interpreted as the probability to find a quark with a co-linear (along the direction of the momentum transfer from the probe) momentum fraction x in a hadron. However, the one-dimensional momentum distributions don't tell the full story of what's happening inside the hadron, and during the last 15-20 years the focus has shifted to the study of three-dimensional nucleon structure.

The transverse momentum dependent parton distribution functions (TMDs) are a set of functions $f(x, \boldsymbol{k}_T)$ that describe quark distributions for a quark with momentum fraction x and a momentum in the transverse plane $\boldsymbol{k}_T$. TMD functions are expected to be universal, and show up in the cross sections for Drell-Yan ($hh \to l\bar{l}X$) and semi-inclusive deep inelastic scattering (SIDIS) and other processes. This thesis work will measure SIDIS.

At leading order (twist two) there are eight TMD functions, each corresponding to different combinations of quark and nucleon spin. They are shown in figure **??**. The Boer-Mulders function $h_1^\perp$ for example, describes the difference in transverse quark polarization in an unpolarized nucleus. A non-zero observation of the Boer-Mulders function would imply that quarks have a non-zero orbital angular momentum. The measurement of $F_{UU}^{\cos\phi}$, and $F_{UU}^{\cos(2\phi)}$ provide data which can be used to test model dependent predictions for the Boer-Mulders function, as well as any future predictions for the structure functions (these need not even be related to the TMD framework).

1.3 Quantitative Motivation

Deep Inelastic Scattering (DIS) events are those in which a lepton $e(l)$ collides with a hadron $h(P)$ (in our case a proton), transferring sufficient momentum (sufficiently is an imprecise term, as a working assumption I use $Q^2 \geq 1.0 \, GeV^2/c^2$) to the hadron to interact with one of it's constituent partons. An inclusive event is one in which only the outgoing lepton is identified and the kinematics are calculated based on the difference between the beam leptons and the final state lepton. Semi-Inclusive DIS (SIDIS) events are those in which one (or more) hadron is detected in the final state along with the scattered lepton $e'(l')$.

"Leading-Twist" *TMD* Quark Distributions

Quark \ Nucleon	Unpol.	Long.	Trans.
Unpol.	f_1 = ⬤		$f_{1T}^{\perp}$ = ⬤ − ⬤
Long.		g_{1L} = ⬤→ − ⬤→	g_{1T} = ⬤ − ⬤
Trans.	$h_1^{\perp}$ = ⬤ − ⬤	$h_{1L}^{\perp}$ = ⬤→ − ⬤→	h_{1T} = ⬤ − ⬤ ; $h_{1T}^{\perp}$ = ⬤ − ⬤

Figure 1: Leading twist TMD PDFs and their interpretation in terms of different combinations of quark/nucleon spin.
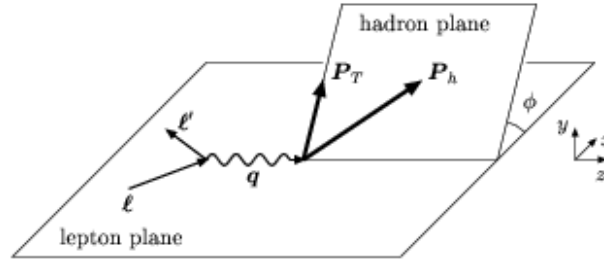
Figure 2: The angle ϕ_h shown as the angle between the lepton and hadron planes in a SIDIS event.

$$e(l) + h(P) \rightarrow e'(l') + h(P_h) + X \tag{1}$$

In SIDIS it is customary to define the following kinematic variables (where $q = l - l'$ and $Q^2 = -q^2$).

$$x = \frac{Q^2}{2P \cdot q} \qquad y = \frac{P \cdot q}{P \cdot l} \qquad z = \frac{P \cdot P_h}{P \cdot q} \qquad \gamma = \frac{2Mx}{Q} \tag{2}$$

Additionally, the ratio ε of the longitudinal and transverse photon flux is shown below.

$$\varepsilon = \frac{1 - y - \frac{1}{4}\gamma^2 y^2}{1 - y + \frac{1}{2}y^2 + \frac{1}{4}\gamma^2 y^2} \tag{3}$$

The differential cross section for the SIDIS reaction $ep \rightarrow ehX$ can be written in a model independent way using a set of structure functions F [1]. The differential cross section, without terms due to polarized targets that are not relevant for this thesis, is given below.

$$\frac{d\sigma^{e^- P \rightarrow e^- hX}}{dx_B \, dQ^2 \, dz \, d\phi_h \, dp_{h\perp}^2} = \frac{\alpha_{em}^2}{2x_B y Q^2} \frac{y^2}{1 - \varepsilon}(1 + \frac{\gamma^2}{2x_B})\Big\{ F_{UU,T} + \varepsilon F_{UU,L}$$
$$+ \sqrt{2\,\varepsilon(1 + \varepsilon)} \cos\phi_h F_{UU}^{\cos\phi_h} + \varepsilon \cos(2\phi_h) F_{UU}^{\cos 2\phi_h} + \lambda_e \sqrt{2\,\varepsilon(1 - \varepsilon)} \sin\phi_h F_{LU}^{\sin\phi_h} \Big\} \tag{4}$$

Here λ_e refers to the helicity of the incoming lepton (beam electron in our case). If one decomposes the hadronic matrix element which is present in the hadronic tensor into different possible Dirac

structures, a set of functions known as transverse momentum dependent parton distributions functions (TMD PDFs) and transverse momentum dependent fragmentation functions (TMD FFs) can be defined. The structure functions from above can then be calculated as a convolution of these more basic non-perturbative functions. The notation $\mathcal{C}$ is shorthand presented in [2] as a way to write structure functions in terms of the convolutions of PDF and FF objects.

$$\mathcal{C}[\omega f D] = x \sum_a e_a^2 \int d^2\boldsymbol{p}_T d^2\boldsymbol{k}_T \delta^{(2)} \left(z\boldsymbol{k}_T + \boldsymbol{p}_T - \boldsymbol{P}_{h\perp}\right) \omega(\boldsymbol{k}_T, \boldsymbol{p}_T) f^a(x, k_T^2) D^a(z, p_T^2) \tag{5}$$

where a is summed over quarks and anti-quarks. The five structure functions appearing in the cross section are,

$$F_{UU,T} = \mathcal{C}[f_1 D_1] = x \sum_a e_a^2 \int d^2\boldsymbol{p}_T d^2\boldsymbol{k}_T \delta^{(2)} \left(z\boldsymbol{k}_T + \boldsymbol{p}_T - \boldsymbol{P}_{h\perp}\right) f_1^a(x, k_T^2) D_1^a(z, p_T^2) \tag{6}$$

$$F_{UU,L} = 0 \tag{7}$$

$$F_{UU}^{\cos\phi_h} = \frac{2M}{Q} \mathcal{C}\left[-\frac{\hat{\boldsymbol{h}} \cdot \boldsymbol{k}_T}{M_h}\left(xhH_1^\perp + \frac{M_h}{M} f_1 \frac{\tilde{D}^\perp}{z}\right) - \frac{\hat{\boldsymbol{h}} \cdot \boldsymbol{p}_T}{M}\left(xf^\perp D_1 + \frac{M_h}{M} h_1^\perp \frac{\tilde{H}}{z}\right)\right] \tag{8}$$

$$F_{UU}^{\cos 2\phi_h} = \mathcal{C}\left[-\frac{2(\hat{\boldsymbol{h}} \cdot \boldsymbol{k}_T)(\hat{\boldsymbol{h}} \cdot \boldsymbol{p}_T) - \boldsymbol{k}_T \cdot \boldsymbol{p}_T}{MM_h} h_1^\perp H_1^\perp\right] \tag{9}$$

$$F_{LU}^{\sin\phi} = \frac{2M}{Q} \mathcal{C}\left[-\frac{\hat{\boldsymbol{h}} \cdot \boldsymbol{k}_T}{M_h}\left(xeH_1^\perp + \frac{M_h}{M} f_1 \frac{\tilde{G}^\perp}{z}\right) + \frac{\hat{\boldsymbol{h}} \cdot \boldsymbol{p}_T}{M}\left(xg^\perp D_1 + \frac{M_h}{M} h_1^\perp \frac{\tilde{E}}{z}\right)\right] \tag{10}$$

where the previously mentioned Boer-Mulders function $h_1^\perp$ appears at leading order in the $F_{UU}^{\cos 2\phi_h}$ term. This dissertation will present measurements of combinations of these 5 structure functions. The unpolarized terms which carry UU indices will be accessed directly through the SIDIS cross section, and the $F_{LU}^{\sin\phi_h}$ term will be measured by measuring the beam spin asymmetry. The beam spin asymmetry (BSA) is defined as the cross section difference (with respect to the 2 beam helicity states) over the total cross section.

$$BSA = \frac{d\sigma^+ - d\sigma^-}{d\sigma^+ + d\sigma^-} = \frac{A_{LU}^{\sin\phi} \sin\phi}{1 + A_{UU}^{\cos\phi} \cos\phi + A_{UU}^{\cos(2\phi)} \cos(2\phi)} \tag{11}$$

Where the coefficient $A_{LU}^{\sin\phi}$ is defined as,

$$A_{LU}^{\sin\phi} = \sqrt{2\varepsilon(1-\varepsilon)} \frac{F_{LU}^{\sin\phi}}{F_{UU,T} + \varepsilon F_{UU,L}} \tag{12}$$

This asymmetry is particularly interesting because all of the terms that appear in the expansion of the structure function have a pure twist-3 contribution. If the measurement of this BSA is therefore non-zero, it indicates a sizable contribution of twist-3 TMD functions. This effect has been observed to be non-zero previously for π mesons in the work of [3].
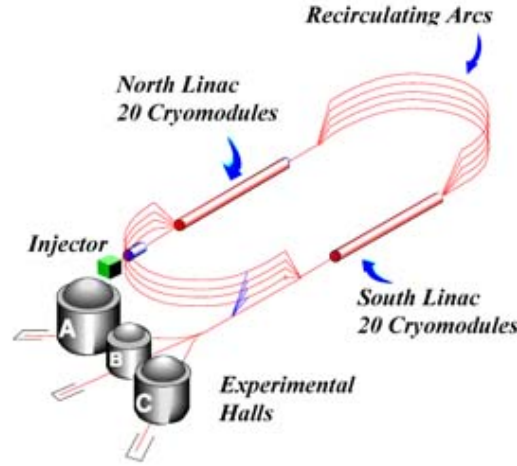
Figure 1: Layout of CEBAF.

Figure 3: Diagram showing how CEBAF is constructed.

2 Methodology

To measure the SIDIS events, one needs a source of high energy electrons, a detector system capable of measuring the final state electron and hadron, and a computing cluster to perform data processing and analysis. This section details the methodology that is and will be used to complete this thesis.

2.1 Experimental Facility

Jefferson Lab is home to the Continuous Electron Beam Accelerator Facility (CEBAF) [4]. It houses 4 state of the art experimental end-stations for fixed target collisions of electrons or photons on various targets. CEBAF begins with a 45-MeV electron injector. The accelerator consists of two linear accelerators (north and south LINACs) and a set of 4 recirculating arcs at both ends of the race track shaped facility. Electrons are passed through the LINACs up to 4 times, gaining 1.14 GeV each pass. CEBAF was designed to generate up to 6 GeV electron beams, and has now been upgraded to provide 12 GeV electrons. Bunches of approximately 1 million electrons are delivered to the halls at 2 nanosecond intervals.

2.1.1 CLAS in Hall-B

Hall-B contains the CEBAF Large Acceptance Spectrometer (CLAS) a large spherical detector capable of measuring final state particles with a large range of momentum and angles. CLAS has the ability to measure exclusive reactions, reconstructing the 4-vectors of all final state particles involved in the reaction. In cases where one particle is not detected, CLAS also has the resolution to resolve them from missing mass spectra. This is achieved by combining several different types of detectors into one package, which will be described below. The CLAS detector has now been dismantled and replaced with CLAS12, but the following sections describe CLAS as it was at the time of data taking for the E1-F experiment used in this thesis. The major components of CLAS [5] are designed to identify different types of particles at different ranges of momenta, they are:

- Large Torus Magnet - The torus is the central bending magnet which creates a toroidal magnetic field and dictates the design of almost all other detectors. The torus consists of 6 superconducting coils, (operated at up to 3860 Amperes) which separate the forward detector systems into 6 distinct sectors. The torus magnet can be used to bend charged particles toward or away from the beamline, and creates the field necessary to determine charge and momentum of particles incident on the CLAS detectors.
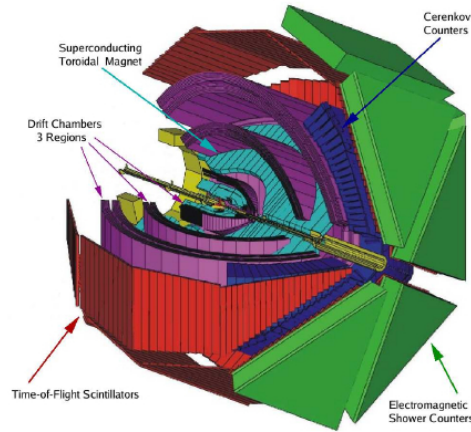
Figure 4: Computer Rendering of CLAS with detector subsystems labeled.

- Drift Chamber systems - A total of 18 drift chambers are used, 3 radially separated chambers per sector which are referred to as "Regions 1-3". The primary role of the drift chambers is to provide charge identification and momentum by measuring the bend of the particle as it passes through the known magnetic field.

- Cherenkov Light Counters - CLAS is equipped with 6 Cherenkov light counters, filled with C_4F_{10}. The Cherenkov Counters (CC) serve two purposes. The CC serves as a trigger for electrons, and also separates electrons from negative pi-mesons π^- below 2.5 GeV/c.

- Scintillating Time Of Flight Panels - Scintillating time of flight (TOF) counters offer coverage from $8° - 142°$ in the polar angle. The primary function of the TOF system is to provide timing information to differentiate between particles of different mass based on their time of flight and momentum.

- Electromagnetic Calorimeter - The last layer of detection is the electromagnetic calorimeter (EC), which consists of alternating layers of lead and scintillation material. Electrons and photons can be detected from the shower they leave behind as they pass through the EC. The EC was designed to have a layered structure, so as to provide hit position information as the particle passes through each layer. The EC is vital in reconstructing neutrals which decay into photons (such as π^0, η).

2.2 Data Analysis

Analysis of the data taken by the CLAS detector is a process which starts with reconstruction of the raw data (electrical signals recorded by ADC and TDC components). The reconstruction algorithm builds particle tracks by finding the best possible track through a set of detector hits. The result is a set of files with charge, momentum, timing, and preliminary particle identification information for each event. The reconstruction package is the critical first step to a data analysis, however the first task for most analyst's is the identification of electrons.

2.2.1 Electron Identification

All negative tracks start out as electron candidates, they are accepted if they pass a series of identification cuts. The ratio E_{dep}/p is calculated for each track, and because electrons have a very constant ratio as a function of momentum, we can use this ratio to separate them from minimally ionizing particles (π^- being the most dominant background). Exploiting this same logic, a cut is placed on the minimum energy deposited in the electromagnetic calorimeter inner layers.Tracks that pass these cuts are next subjected to a variety of geometric cuts to ensure that they pass through regions of the detectors that are well understood. Tracks passing too close to the edges of the electromagnetic calorimeters can shower outside of the detector leading to incorrect reconstruction of energy for that particle. Finally, cuts are applied to the Cherenkov counter signal. Often, charged pions do not have enough momentum
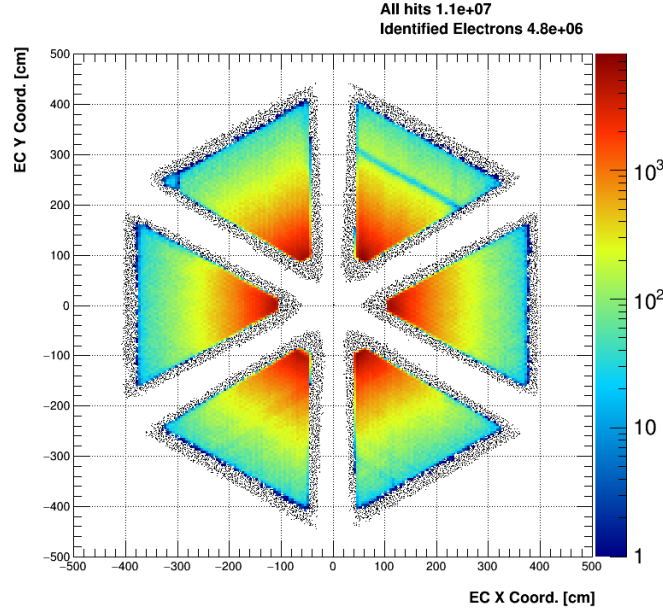
Figure 5: Electromagnetic (EC) calorimeter negative track hits. Shown in black, negatives tracks rejected in electron identification. Hits close to the borders of the EC incompletely shower and can reconstruct with incorrect energy.

$p \leq 2.4\ GeV/c$ to participate in the Cherenkov Effect and no signal is preset in the Cherekov Counter. By requiring a signal in the Cherenkov we remove these events. We then apply matching cuts to the detection angle of the track in the Cherenkov Counter and the number of the PMT which detected the track (these should be 1-to-1 correlated). These procedures are described in detail in my dissertation.

2.2.2 Kaon Identification

If an event contains a good electron, the rest of the event is processed. Kaons are identified based on time of flight information. In this analysis, we use a maximum likelihood ratio technique to classify all positive tracks as either pions, kaons, or protons. Finally, we control the track quality by requiring a significance level of $\alpha = 0.05$.

2.3 EVA Framework

The Evaluation and VAlidation (EVA) software is a project on-going at the University of Connecticut and Jefferson Lab. The goal of EVA is to build a tool that can be used to extract TMD functions from data taken during CLAS12 operation, as well as global data from other collaborations/experiments. As a form of validation, EVA will have the ability to generate physics events based on some physics model and a set of parameters. These events can be fed into the particle swimming detector simulation for CLAS12, and the results can be analyzed. The EVA framework can then extract from the simulated data the parameters in the chosen model. These parameters can be compared with the starting point in the EVA chain.

The cross section results will be used in the EVA framework to test the compatibility of this data with current models with and without inclusion of a twist-4 Cahn term.

3 Analysis of Inclusive Cross Section

The structure function ratios $A_{UU}^{\cos\phi}$ and $A_{UU}^{\cos(2\phi)}$ were previously measured by hall-B and analyzed by Nathan Harrison. In this dissertation we extend this previous work by calculating, validating, and applying the integrated luminosity factor necessary to transform this previous measurement into an absolute cross section. In order to validate the integrated luminosity calculation, we have measured the cross section for inclusive electron scattering ($ep \to e'X$). This work entailed calculating the integrated luminosity [?], measuring the electron yield in bins of W and Q^2, and corrected these yields for acceptance effects as well as radiative effects. The cross section is experimentally measured by combining the following factors.

$$\frac{d\sigma_i}{dWdQ^2} = \frac{1}{\Delta W_i \Delta Q_i^2} \frac{N_{obs} - N_{BG}}{\mathcal{L}} \frac{1}{A_i R_i} \tag{13}$$

Here W is the invariant mass of the virtual photon and target system ($\gamma^* + p$), calculated as $W = \sqrt{M_p^2 - Q^2 + 2p^\mu q_\mu}$. In the equation above, A_i, and R_i refer to the acceptance and radiative correction in the $i - th$ bin. This cross section is experimentally well studied, and our comparison with existing models shows that our measurement is consistent. This gives us a trust in our electron identification, as well as our luminosity (used later to scale the SIDIS data). The inclusive scattering measurement will be described below.

3.1 Calculation of Integrated Luminosity

During running of experimental data taking beam charge accumulates on the Faraday Cup. The accumulated charge is written out into the data files for later processing. By summing the charge on the Faraday cup over the entire set of files used in the analysis, the total accumulated charge ΔQ can be calculated. The incoming number of electrons is then $N_e = \Delta Q/e$. The integrated luminosity is then;

$$\mathcal{L} = \frac{\Delta Q l_t \rho}{e} \tag{14}$$

Care is taken when calculating the integrated luminosity. In the case that there is a time period where charge is accumulating and events are not, this section is skimmed out of the datafile, and the charge is not added. In the case that there is no charge accumulating but events are occuring, these events are discarded.

3.2 Acceptance Corrections

A fraction of the events which occur are not captured by the detector due to two main reason:

1. The detector components do not have 100% efficiency.

2. The detector has geometric holes and obstructions, through which particles can/can not pass.

Some of these effects (holes/obstructions) can be taken into consideration using fiducial cuts during the particle identification stage. Other effects have to be taken into account by correcting for the detectors not perfect acceptance. This is done by creating a computer model of the detector, as realistically as possible. Inclusive events (with radiative effects) are then simulated leaving the target and propagating through the magnetic field, hitting the detectors of CLAS. These results can then be used to form the correction factor $A = N_{rec}/N_{gen}$ in every bin.

3.3 Radiative Corrections

It is not uncommon for electrons to emit a real photon in the initial or final state of the interaction. These radiations alter the event kinematics and must be removed in order to present Born cross sections (nature provides us with the radiated cross section). This is done by modeling the inclusive reaction with and without radiative effects and comparing the results. The correction factor $R = N_{rad}/N_{norad}$ can be constructed from a sufficient event generator(in this analysis we use `keppel_rad` and `keppel_norad`).
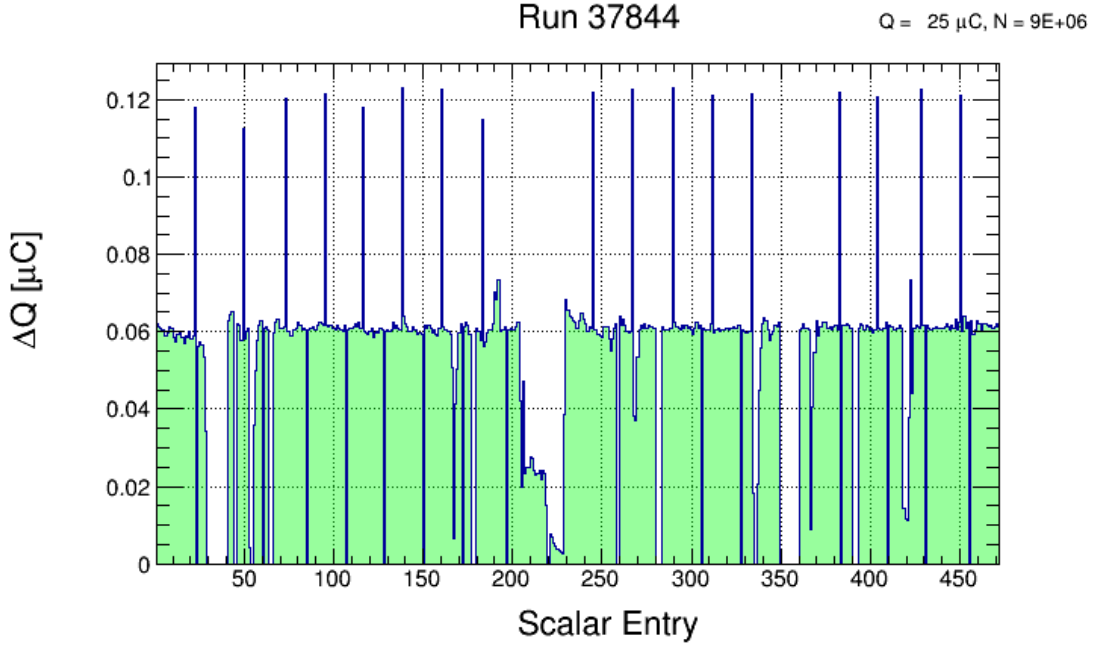
Figure 6: The charge accumulated per scalar entry for run 37844.

3.4 Comparison to Model

Our result is compared to a parametrization of the resonance region between $W \in [1.1, 2.0]$ [6]. This parametrization was originally developed by Cynthia Keppel (using SLAC data) and has been improved using data from Hall-C over time. Over the majority of the kinematics the result is within 5% of the model value. This contamination is in large part due to elastic events which persist in the lower and higher W parts of the measurement. Despite this, the average discrepancy over the entire phase-space of the measurement is included as a quoted uncertainty on the integrated luminosity.
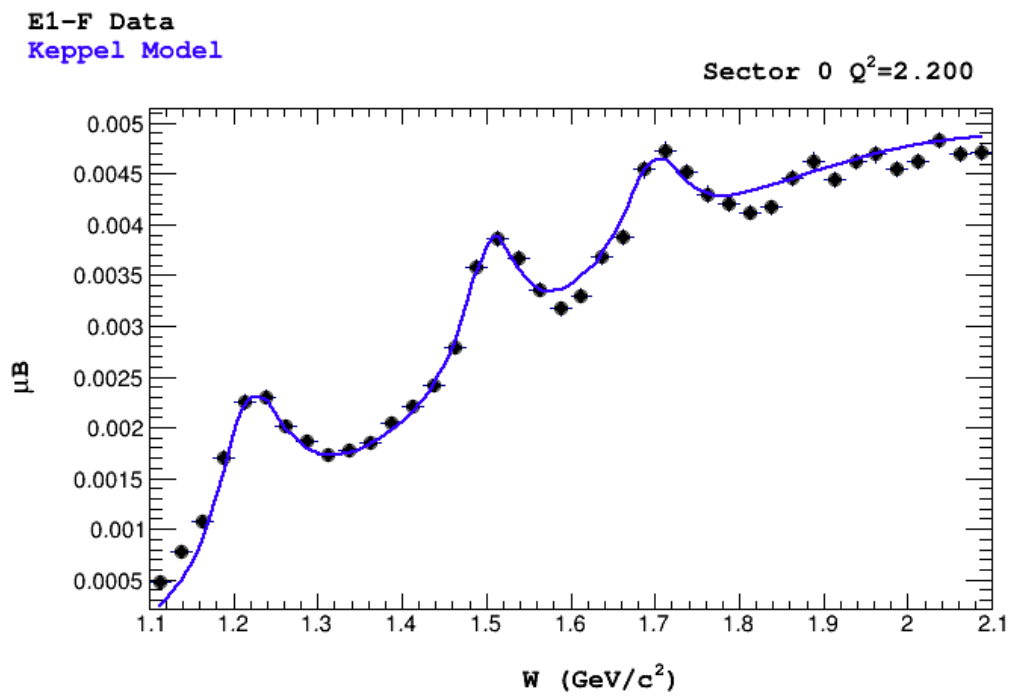
E1-F Data
Keppel Model

Sector 0 Q^2=2.200

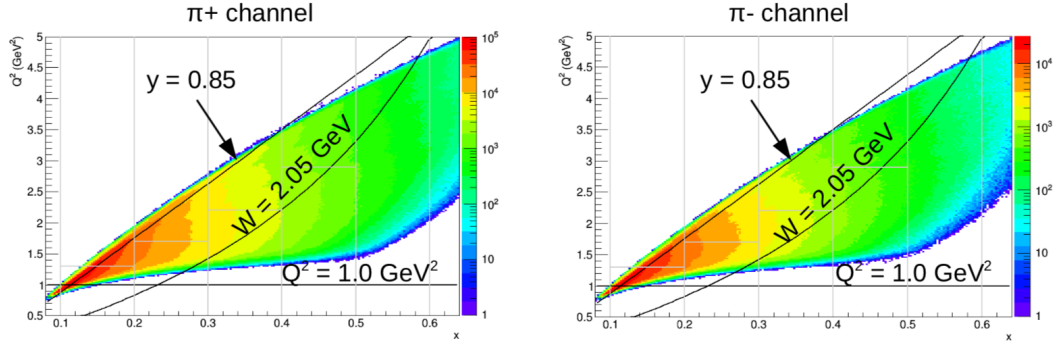Figure 7: Our cross section result compared with Keppel's model.

Figure 8: Kinematic coverage for x and Q^2 shown for both charged pions. The binning described above for x and Q^2 is overlaid in gray. Figure credit to Nathan Harrison [7].
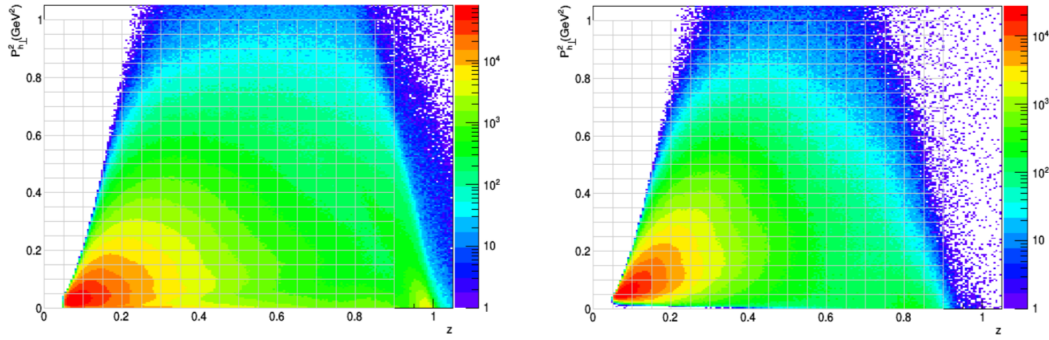

Figure 9: Kinematic coverage for z_h and P_T^2 shown for both charged pions (left π^+ and right π^-). Figure credit to Nathan Harrison [7].

4   Semi-Inclusive DIS

Multiplicities for unpolarized pion SIDIS have been provided by HERMES and COMPASS, however no measurement has been made of the absolute cross section. In this section, a collaborative effort between the author and Nathan Harrison is described that will produce the differential cross section for $\pi^\pm$ SIDIS at JLab kinematics.

Using the E1-F dataset we have identified all events which contain a good electron and a charged pion. These events are measured fully differentially in 5-D binning of x, Q^2, z_h, P_T^2, and ϕ_h. Events are binned in the same way for both π^+ and π^-. Five equal sized bins are chosen in x, and each x bin contains 2 bins of Q^2 (except for the highest x bin). The split in Q^2 depends on the x value, increasing with increasing x (1.3, 1.7, 2.2, 2.9). The hadronic variables are binned in a simple manner, with 18 z_h bins between 0-0.9, 20 P_T^2 bins between 0.0 and 1.0 GeV^2/c^2. Finally ϕ_h is binned into 36 equal sized bins that span the full 360 degree range.

Acceptance corrections are applied in the same way described in the inclusive section, in this case a Pythia based model is used to generate events. The kinematic dependence of the reconstructed events matches well with the data, except for the ϕ_h axis where an iterative procedure is used to find suitable initial parameters for $A_{UU}^{\cos\phi_h}$ and $A_{UU}^{\cos(2\phi_h)}$.

Radiative corrections are produced using HAPRAD 2.0, which takes the Born cross section (produced by a model) and produces the radiated cross section. This procedure is discussed in more detail in the dissertation document.
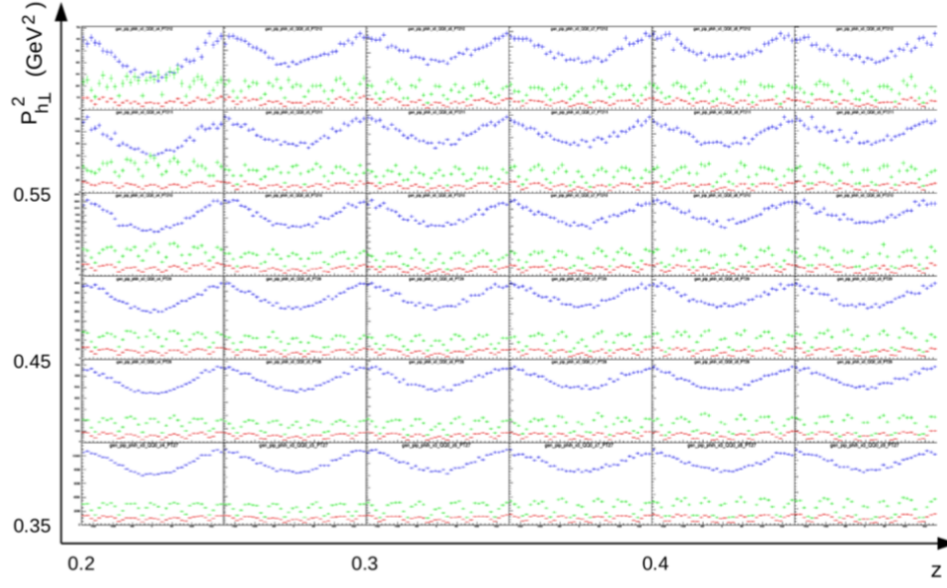
11

Figure 10: Acceptance for bins of z_h, P_T^2 as a function of ϕ_h shown in green for π^+. Generated events appear here in blue, and reconstructed events in red. Figure credit to Nathan Harrison [7].
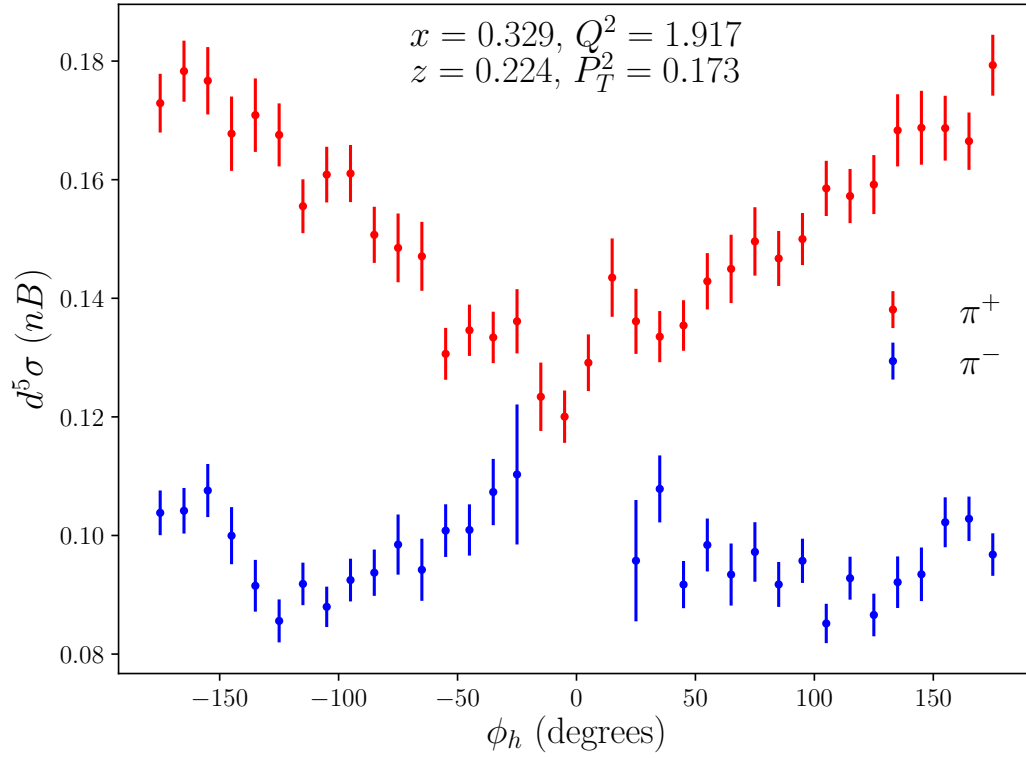

Figure 11: The 5-dimensional cross sections are shown for both charged pions, this figure is a preliminary result of our study. The quoted kinematic point is the center of the bin of measurement.

5 Kaon Beam Spin Asymmetry

In addition to the unpolarized structure functions which will be accessible from the SIDIS cross section measurement, the beam spin asymmetry for positively charged k-mesons in SIDIS is measured. This gives us access to an additional structure function $F_{LU}^{\sin\phi}$. The measurement was performed as a function of ϕ_h and 4 different kinematic variables x, Q^2, z, and P_T.

In order to measure kaons in the kinematically accepted DIS region, we exclude events with have $Q^2 < 1 GeV^2/c^2$ or which have $W < 2\ GeV/c^2$. Additionally when measuring the axes (x, Q^2, and P_T), the range of z values included in the sample is limited to be within 0.25-0.75. This cut is used as an attempt to make our measurement in the current fragmentation region where factorization has been proved.

5.1 Helicity Determination

The beam helicity is measured periodically with a Moller polarimeter. These measurements were analyzed statistically by Wes Gohn and it was observed that the average beam polarization was 75%, with a variance of approximately 1%.

5.2 Measurement of ϕ Dependent Asymmetry

After the final sample of events has been selected, the events are binned in 12 bins of ϕ and 10 bins of the kinematic axis. The calculation of the BSA in each bin is done.

$$A = \frac{1}{P_e} \frac{\Delta N}{N} \tag{15}$$

Here P_e is the fractional polarization of the beam (explained above), $N = N_+ + N_-$ and, $\Delta N = N_+ - N_-$. By using error propagation and assuming the statistical error on the counts N to be $\sqrt{N}$ one can show that the uncertainty in the beam spin asymmetry due to the statistical uncertainty in the counts is,

$$\sigma_A^2 \approx \frac{A^2}{P_e^2}\sigma_{P_e}^2 + \frac{4}{P_e^2(N_+ + N_-)^4}(N_-^2\sigma_{N_-}^2 + N_+^2\sigma_{N_+}^2) \tag{16}$$

where the uncertainty due to the P_e will be added to the systematic errors. The counts are taken to be drawn from a Poisson distribution (which describes the probability to observe ν events when you expect N). The variance on the counts is equal to the mean (N). The statistical errors are then quoted as shown below.

$$\sigma_A^2 \approx \frac{4N_+ N_-}{P_e^2(N_+ + N_-)^3} \tag{17}$$

5.3 Systematic Uncertainties

The value of the measurement of the beam spin asymmetry in each bin can be influenced by many factors. Common examples include the particle identification routines, the subtraction of backgrounds, and the calibration (mis-calibration) of detectors. A mis-calibrated detector represents a systematic effect, that consistently moves the measured value one direction or another. These effects are corrected for, and the detector calibration is adjusted or fixed. In this way I have attempted to eliminate all systematic effects. The degree of uncertainty which remains as to my ability to correct for a systematic effect, I call systematic uncertainty.

First the contribution to the total systematic uncertainty which comes from the uncertainty in the measured value of the beam polarization is considered. This contribution is combined together with other sources of systematic uncertainty, such as the uncertainty on input parameters to the analysis code. The complete procedure for handling systematic uncertainties will be described in the thesis work, and my final estimates will be tabulated. My current estimates are shown as red bars in the figure below.
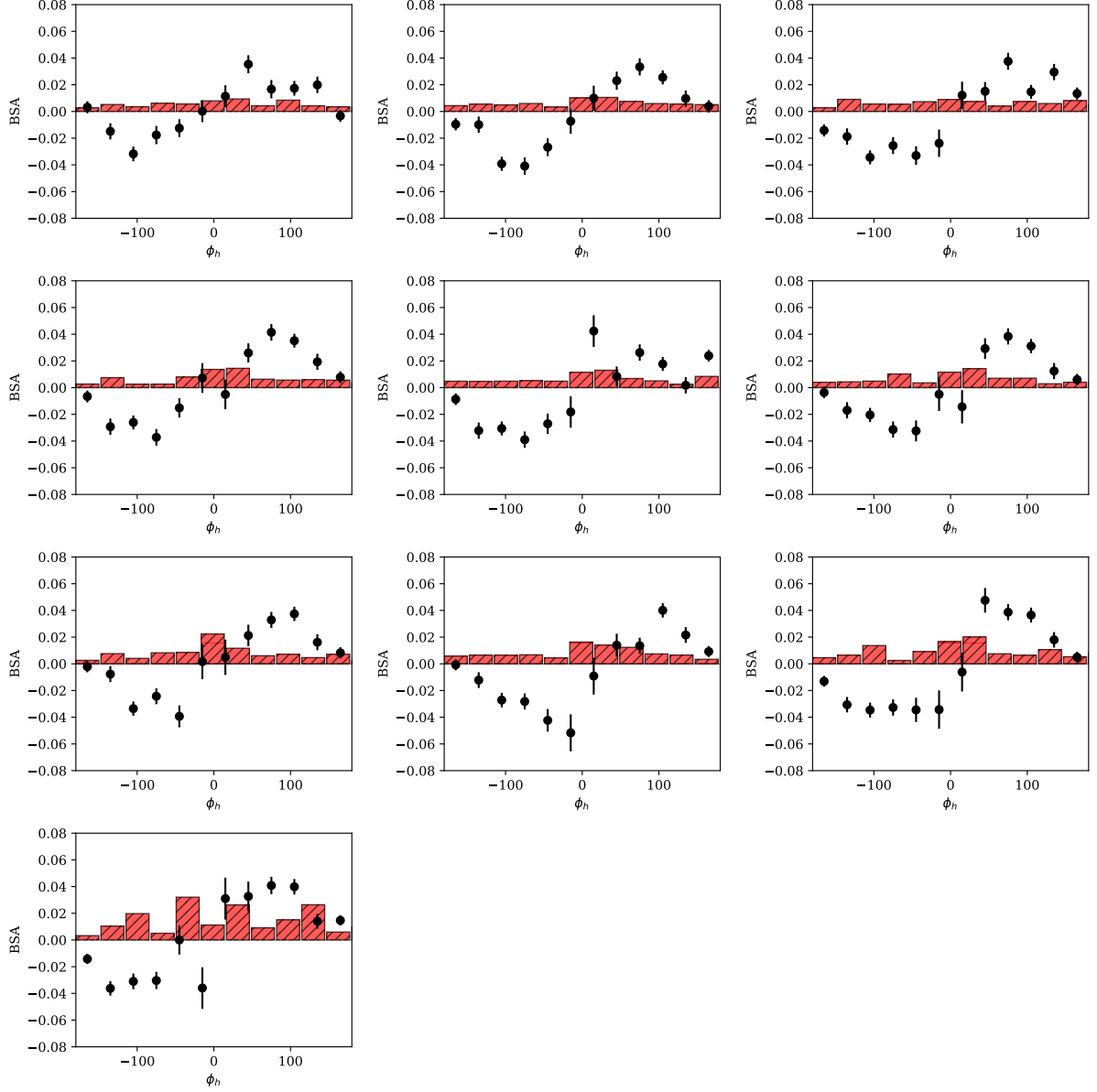
Figure 12: The beam spin asymmetry as a function of ϕ_h between -180 and 180 degrees shown for 10 bins of z_h, increasing from top left to bottom right.

5.4   Conclusion and Outlook

We have extracted integrated beam spin asymmetry measurements for four different kinematic variables. In doing so, we observe non-zero contributions from twist-3 (or higher) TMD/FF functions. Our measurement can now be studied using phenomenological models of TMD and FF distributions. To conclude this project we will provide systematic uncertainties for the extracted modulations, and compare it to a phenomenological model.

6   Conclusion and Outlook

In this document, I have described my ongoing research efforts to make an impact in the field of nucleon structure research. Specifically, we propose that this dissertation project will (1) extract the structure function $F_{LU}^{\sin\phi}$ for positive kaons, (2) take steps necessary to extend a current CLAS measurement of unpolarized SIDIS azimuthal modulations to the absolute (SIDIS) cross section, and (3) utilize existing phenomenology and modeling to predict these measurements. My work on both (1) and (3) is now at an advanced stage, and the remaining tasks have been briefly described in the document above.

References

[1] P. J. Mulders and R. D. Tangerman, Nucl. Phys. **B461**, 197 (1996), [Erratum: Nucl. Phys.B484,538(1997)], arXiv:hep-ph/9510301 [hep-ph] .

[2] A. Bacchetta, M. Diehl, K. Goeke, A. Metz, P. J. Mulders, and M. Schlegel, JHEP **02**, 093 (2007), arXiv:hep-ph/0611265 [hep-ph] .

[3] W. Gohn *et al.* (CLAS), Phys. Rev. **D89**, 072011 (2014), arXiv:1402.4097 [hep-ex] .

[4] C. W. Leemann *et al.*, Ann. Rev. Nucl. Part. Sci. **51**, 413 (2001).

[5] B. A. Mecking *et al.* (CLAS), Nucl. Instrum. Meth. **A503**, 513 (2003).

[6] C. Keppel, *Inclusive nucleon resonance electroproduction at large momentum transfer*, Ph.D. thesis, American U. (1994).

[7] N. A. Harrison, *Exploring the Structure of the Proton via Semi-Inclusive Pion Electroproduction*, Ph.D. thesis, Connecticut U. (2010).